CMS Physics Analysis Summary

Contact: cms-pag-conveners-exotica@cern.ch 2015/05/29

Search for long-lived, neutral particles decaying to photons

The CMS Collaboration

Abstract

A search is performed for long-lived neutral particles decaying to photons and invisible particles. An example of a physics process leading to such a signature is the decay of the lightest neutralino with nonzero lifetime into a gravitino and a photon, as predicted by gauge-mediated supersymmetric models. The search is based on events containing at least two photons of which at least one has converted to an e^+e^- pair, at least two jets, and missing transverse energy. The transverse impact parameter can be reconstructed using photons converting into e^+e^- pairs. We consider scenarios in which the neutralino has a mean lifetime between $c\tau = 0.4$ and 100 cm. The analysis was performed on a data sample collected by the CMS experiment at the LHC in 2012 at center-of-mass energy $\sqrt{s} = 8$ TeV and corresponds to an integrated luminosity of 19.7 fb^{-1} of proton–proton collisions.

1 Introduction

The existence of new, heavy particles with long lifetimes is predicted by many models of physics beyond the standard model (SM), such as hidden valley scenarios [1] or supersymmetry (SUSY) with gauge-mediated SUSY breaking (GMSB) [2]. Under the assumption of R-parity conservation [3], strongly interacting SUSY particles can be pair-produced at the Large Hadron Collider (LHC). Their subsequent decay chain may include one or more quarks and gluons, as well as the lightest SUSY particle (LSP), which escapes detection, giving rise to apparent momentum imbalance in the transverse plane. A GMSB benchmark scenario, commonly described as "Snowmass Points and Slopes 8" (SPS8) [4] is used as reference in this search. In this scenario, the lightest neutralino ($\widetilde{\chi}_1^0$) is the next-to-lightest SUSY particle, and can be long-lived. It decays to a photon (or Z/Higgs bosons) and a gravitino ($\widetilde{\mathrm{G}}$), which is the LSP [5]. If the $\widetilde{\chi}_1^0$ consists predominantly of the bino, the superpartner of the $U(1)$ gauge field, its branching fraction to a photon and $\widetilde{\mathrm{G}}$ is expected to be large.

The signature of these decays is extremely clean since it is given by displaced decay vertices and significant missing energy. As such it is optimal for discovering new physics since the $\widetilde{\chi}_1^0$ has so far been mainly sought after at the CMS experiment assuming that they are short-lived [6]. Figure 1 shows two possible diagrams of squark and gluino pair-production processes that result in a diphoton final state. Similar searches using the photon shower direction (D0 experiment [7]) or time-of-flight with the electromagnetic calorimeter (ATLAS [8, 9], CDF [10], and CMS [11]) have been performed under the assumption of a sufficiently long $\widetilde{\chi}_1^0$ lifetime and have all found no evidence for these signatures of interest.

In this paper, we present the results of a search for long-lived neutral particles decaying to photons obtained with a technique already used in a previous CMS analysis performed at 7 TeV [12]. A photon produced in the decay of a long-lived $\widetilde{\chi}_1^0$ will originate from a displaced vertex with a large absolute transverse impact parameter, $|d_{\mathrm{XY}}|$. In this analysis, reconstructed photon conversions are exploited to determine the photon direction with respect to the beam axis and to measure the $|d_{\mathrm{XY}}|$. The larger the $\widetilde{\chi}_1^0$ lifetime, the wider the distribution of the $|d_{\mathrm{XY}}|$. The strategy consists of selecting events with at least two photons of which at least one has converted to an e^+e^- pair. The $|d_{\mathrm{XY}}|$ distribution is then used to search for an excess of signal over SM background events. Moreover, in this and many other SUSY models that assume the conservation of R-parity, the $\widetilde{\chi}_1^0$ is produced in association with high transverse momentum (p_{T}) jets and significant missing transverse energy ($E_{\mathrm{T}}^{\mathrm{miss}}$) from the LSP. For this search, we consider scenarios in which the neutralino has a mean lifetime between $c\tau = 0.4$ and 100 cm.

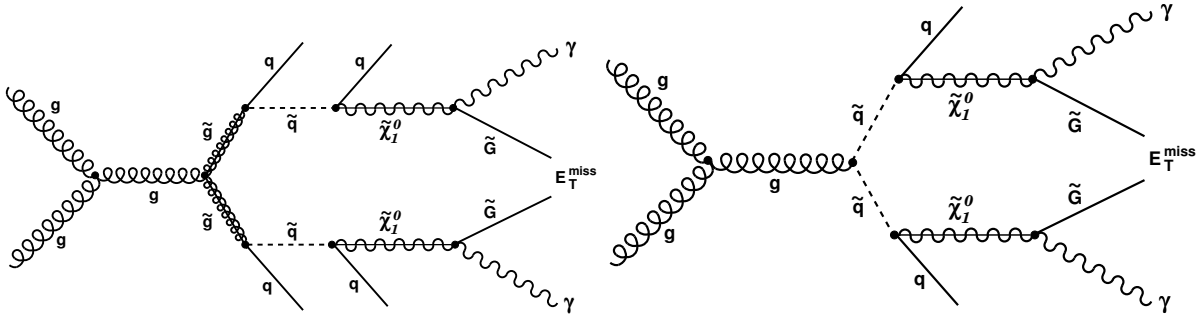

Figure 1: Feynman diagrams for SUSY processes that result in a diphoton-plus-$E_{\mathrm{T}}^{\mathrm{miss}}$ final state through squark-mediated (left) and gluino-mediated (right) production at the LHC.

2 CMS Detector

A more detailed description of the CMS detector, together with a definition of the coordinate system used and the relevant kinematic variables, can be found in Ref. [13]. The central feature of the CMS apparatus is a superconducting solenoid with an internal diameter of 6 m, providing a magnetic field of 3.8 T. Within the superconducting solenoid volume there are the silicon pixel and strip trackers, a lead tungstate crystal electromagnetic calorimeter (ECAL), and a brass plus scintillator hadron calorimeter (HCAL), each composed of a barrel and two endcap sections. Muons are detected by gas-ionization detectors embedded in the steel flux-return yoke outside the solenoid. Extensive forward calorimetry complements the coverage provided by the barrel and endcap detectors. The energy resolution for photons with $E_{\mathrm{T}}\approx$60 GeV varies between 1.1% and 2.6% over the solid angle of the ECAL barrel, and from 2.2% to 5% in the endcaps [14]. The silicon tracker measures charged particles within the pseudorapidity range $|\eta| < 2.5$. It consists of 1440 silicon pixel and 15 148 silicon strip detector modules and is located in the 3.8 T field of the superconducting solenoid. For nonisolated particles of $1 < p_{\mathrm{T}} < 10$ GeV and $|\eta| < 1.4$, the track resolutions are typically 1.5% in p_{T} and 25–90 (45–150) μm in the transverse (longitudinal) impact parameter [15].

3 Samples

The data samples used for this analysis were collected in 2012 by the CMS detector [13] at the LHC from proton–proton collisions at a center-of-mass energy of 8 TeV, corresponding to an integrated luminosity of 19.7 fb^{-1}. The data sample is used both for the selection of signal candidates and for control samples used for data-driven background estimation. Events are selected using a trigger that requires at least two photons with $p_{\mathrm{T}} > 40$ GeV and $|\eta| < 2.4$.

Simulated samples for the signal processes are generated for a range of $\widetilde{\chi}_1^0$ mass hypotheses between 200 and 260 GeV, and mean $\widetilde{\chi}_1^0$ lifetimes between $c\tau = 0.4$ and 100 cm to target regions of phase space not already excluded by a previous search [11]. The simulation uses the PYTHIA 6.4 event generator [16], with the CMS detector response fully simulated using GEANT4 [17]. Due to the high luminosities attained during the run, many events have multiple proton–proton interactions leading to a distribution of primary vertices referred to as pileup. The generated pileup distribution in the simulated samples was reweighted to reproduce the 2012 data-taking conditions.

4 Object reconstruction and event selection

The particle-flow (PF) event algorithm is used to reconstruct and identify each individual particle with an optimised combination of information from the various elements of the CMS detector. The energy of photons is directly obtained from the ECAL measurement, corrected for zero-suppression effects. The energy of electrons is determined from a combination of the electron momentum at the primary interaction vertex as determined by the tracker, the energy of the corresponding ECAL cluster, and the energy sum of all bremsstrahlung photons spatially compatible with originating from the electron track. The energy of charged hadrons is determined from a combination of their momentum measured in the tracker and the matching ECAL and HCAL energy deposits, corrected for zero-suppression effects and for the response function of the calorimeters to hadronic showers.

Jets are reconstructed using the anti-k_{T} clustering algorithm [18] with distance parameter of $R = \sqrt{(\Delta\eta)^2 + (\Delta\phi)^2} = 0.5$. The inputs to the jet clustering algorithm are the four-momentum

vectors of the reconstructed particles, where each particle is reconstructed with the PF technique. Furthermore, jet candidates are rejected if they are found within $\Delta R = 0.25$ of a photon.

This analysis selects at least two high-p_T isolated photons in association with at least two jets and E_T^{miss} . The two jets are required to have $|\eta| \leq 2.6$ and $p_T > 35\,\text{GeV}$. The photon isolation is defined by summing the transverse momenta of charged hadrons, photons, and neutral hadrons, inside a region with radius ΔR in the (η, ϕ) plane around the photon direction. Since the reconstruction of the signal photons and the PF objects is not optimally synchronised at the time of writing this document, energy from the signal photon must be removed from the isolation sums by imposing geometrical requirements. When calculating the photon isolation, PF photons falling in a pseudorapidity slice of size $\Delta\eta = 0.015$ are excluded from the sum. Similarly, when constructing the neutral hadron isolation, summing the transverse momenta of charged hadrons, a region of $\Delta R = 0.02$ is excluded. The isolation requirements for our selected photons are: $\sum E_{\text{Photon}} < 0.005 \cdot E_T + 1.3\,\text{GeV}$; $\sum E_{\text{Neutral Hadron}} < 0.04 \cdot E_T + 3.5\,\text{GeV}$; $\sum E_{\text{Charged Hadron}} < 2.6\,\text{GeV}$. The cone size for all isolation sums is $\Delta R = 0.3$. The lateral extension of the shower, $\sigma_{\eta\eta}$, is measured in terms of the energy weighted spread within the 5 $\times$ 5 crystal matrix centered on the crystal with the largest energy deposit in the supercluster. Another shower shape variable, S_{Minor}, is defined as the minor axis of the ellipse from the energy deposit in the ECAL. The requirements from $\sigma_{\eta\eta}$ and S_{Minor} are used to ensure that the candidate is consistent with the shape expected from a real photon and reduces the QCD multijet background substantially. We also define H/E as the sum of the energies of HCAL towers within a cone of size $\Delta R < 0.15$ centered on the supercluster position, divided by the supercluster energy. Using these definitions, we select events in which the photons meet the following criteria: at least two photons in the event where the p_T of leading photon > 85 GeV and all other photons with $p_T > 50$ GeV; $|\eta| < 1.47$; $\sigma_{\eta\eta} < 0.012$; $0.15 < S_{minor} < 0.30$; H/E $<$ 0.05. Lastly, photon candidates are rejected if they are likely to be electrons, as inferred from characteristic patterns of hits in the pixel detector, known as 'pixel seeds', that are matched to candidate EM showers.

Due to the presence of gravitinos, the E_T^{miss} distribution of the signal exhibits long tails, whereas for the main SM backgrounds (where the E_T^{miss} is only due to the finite detector resolution) tends to fall off quickly as shown in Fig. 2. In order to choose our E_T^{miss} requirement we use an exclusion based optimisation, whereby we find the cut which minimises the expected upper limit on the signal cross section. For this minimisation we input the background prediction which will be described in Section 6, and the systematic uncertainties which will be described in Section 7. Subsequently, we find the optimal cut to be $E_T^{miss} > 60\,\text{GeV}$ for all signal points considered.

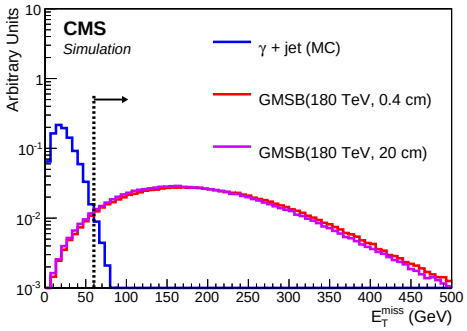

Figure 2: Distribution of E_T^{miss} from simulation for signal and background. All histograms are scaled to unity.

5 Photon conversions and the transverse impact parameter

Electron and positron tracks from photons converting in the material of the silicon tracker are reconstructed [19], and therefore the photon direction can be determined from the track-pair momentum. The extrapolation of the photon direction back to the beam axis then allows us to measure the impact parameter of the photon, $|d_{XY}|$, as shown in Fig. 3. Therefore, we define the $|d_{XY}|$ as the distance of closest approach of the photon trajectory to the beam axis in the transverse plane. Furthermore, the photon trajectory is defined as a straight line from the conversion vertex along the momentum of the e^+e^- pair. Subsequently, for a photon produced in the decay of a long-lived $\tilde{\chi}_1^0$, the extrapolated direction points away from the beam axis giving a sizable $|d_{XY}|$. Also, as mentioned previously, in high luminosity conditions multiple collisions occur within a single bunch crossing producing a number of primary vertices. We therefore measure the $|d_{XY}|$ with respect to the transverse position of the beam axis which is more robust than with respect to the primary vertex considering the presence of pileup vertices.

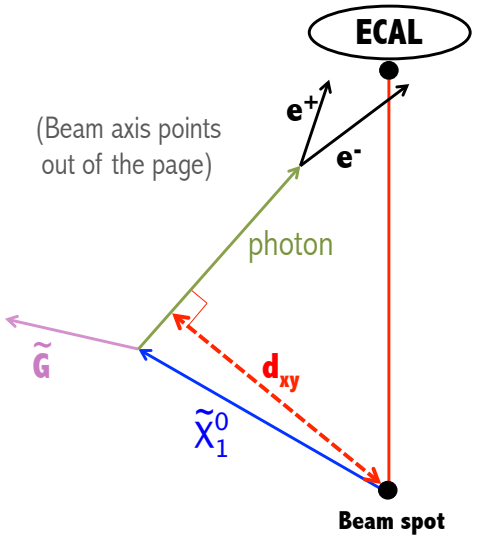

Figure 3: Illustration of the $\tilde{\chi}_1^0 \to \gamma + \tilde{\mathrm{G}}$ decay in the x-y plane with the beam direction coming out of the page. The diagram shows the photon converting to an e^+e^- pair and the subsequent reconstruction of the transverse impact parameter.

6 Background Determination

The main background contribution in this analysis arises from γ+jet events. These events exhibit $E_{\mathrm{T}}^{\mathrm{miss}}$ due to the effect of finite detector resolution (i.e. instrumental $E_{\mathrm{T}}^{\mathrm{miss}}$). In γ+jet events we have typically one real photon and one jet that is misidentified as a photon in the final selection. There are additional sources of background with intrinsic missing transverse energy, such as electroweak processes ($\mathrm{t\bar{t}}$ and W+jets), but these are heavily suppressed by the photon p_{T} requirement and electron veto, and therefore make a negligible contribution to the final selection. The $\tilde{\chi}_1^0 \to \gamma + \tilde{\mathrm{G}}$ decay has two signatures: $E_{\mathrm{T}}^{\mathrm{miss}}$ from the unseen $\tilde{\mathrm{G}}$ and a large $|d_{XY}|$ from the displaced photons. The strategy for determining the background is to use control regions (CRs) in data that are kinematically similar to the signal sample whilst having no real $E_{\mathrm{T}}^{\mathrm{miss}}$; to this purpose, events were selected with $E_{\mathrm{T}}^{\mathrm{miss}} < 30\,\mathrm{GeV}$. The $|d_{XY}|$ background distribution (CR1) is extracted from events with $E_{\mathrm{T}}^{\mathrm{miss}} < 30\,\mathrm{GeV}$ and satisfying all other selection criteria.

To ensure that CR1 gives a good estimation of the background, we compare the $|d_{XY}|$ distribution to the data in the $E_{\mathrm{T}}^{\mathrm{miss}} < 30\,\mathrm{GeV}$ region but failing at least one of the photon isolation requirements in Section 4 (CR2). We also compare to the $|d_{XY}|$ distribution in data for $E_{\mathrm{T}}^{\mathrm{miss}} > 60\,\mathrm{GeV}$ but failing at least one of the photon isolation requirements in Section 4 (CR3). We tabulate the definitions of the various CRs in Fig. 4 for clarity, and show the comparisons in Fig. 5.

	Isolation pass	**Isolation reject**
MET < 30 GeV	CR1	CR2
MET > 60 GeV	Signal Region	CR3

Figure 4: Definition of the background control regions.

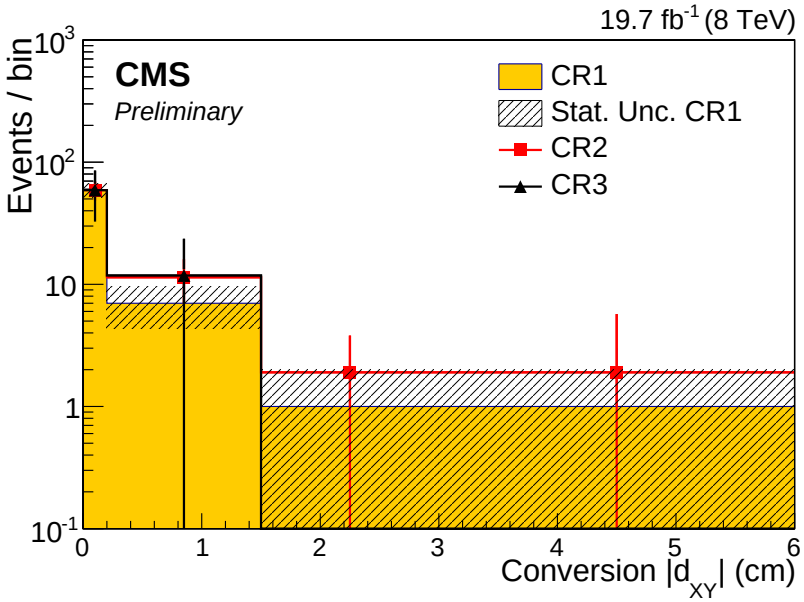

Figure 5: Distribution of $|d_{XY}|$: fake photons from the high $E_{\mathrm{T}}^{\mathrm{miss}}$ region (CR3) and low $E_{\mathrm{T}}^{\mathrm{miss}}$ region (CR2) are compared with real photons from the low $E_{\mathrm{T}}^{\mathrm{miss}}$ region (CR1). The errors are statistical only. The distributions of CR2 and CR3 are normalised to the first bin of CR1.

We see that the $|d_{XY}|$ distributions for our fake photon samples (CR2 and CR3), and real isolated photons (CR1) agree, with the residual differences between the fake and isolated photon distributions in the low $E_{\mathrm{T}}^{\mathrm{miss}}$ control sample consistent within statistical uncertainties. In order to account for this difference between control regions, we take the shape template derived from CR2 as a shape uncertainty on our nominal background estimate (CR1). For the normalisation of CR1, we scale the derived shape template to the peak of the $|d_{XY}|$ distribution in our data (first bin of the histogram).

7 Systematic Uncertainties

A summary of the systematic uncertainties considered affecting the signal efficiency is given in Table 1. The calorimeter response to different types of particles is not perfectly linear and hence corrections are made to properly map the measured jet energy deposition. The uncertainty on

this correction is referred to as the uncertainty on the jet energy scale and varies as a function of position and transverse momentum of the jet [20]. The uncertainty on the photon energy scale is estimated to be 0.6% for barrel photons [21]. The uncertainty on the integrated luminosity is estimated to be 2.6% [22]. A major source of uncertainty on the signal comes from the conversion reconstruction efficiency. The method used to compute this uncertainty is the same as what was performed in Ref. [12], namely to sum in quadrature the difference between the number of reconstructed conversions in data and simulation for $Z \to \mu\mu\gamma$ events; and between $Z \to \mu\mu\gamma$ and the simulated signal. In a mass window of the Z-boson ($60 < m_{\mu\mu\gamma} < 120$ GeV) we look at the percentage of photons that convert, both in data and simulation as performed in Ref. [19] (efficiency = 0.93 ± 0.03). Additionally, we compare the percentage of conversions in the $Z \to \mu\mu\gamma$ (efficiency = 8.5 ± 0.15%) and GMSB simulated samples (efficiencies between 4.7–8.5%). These results are summed in quadrature and set as the systematic uncertainty on the conversion reconstruction efficiency as follows:

$$\begin{aligned} \text{Error} &= \sqrt{(1-0.93)^2 + \left(1 - \tfrac{[4.7 \leftrightarrow 8.5]}{8.5}\right)^2} \\ &= [7 \leftrightarrow 45]\,\%. \end{aligned} \tag{1}$$

Table 1: Systematic uncertainties on the signal efficiency.

Source	Uncertainty (%)
Luminosity	2.6
Statistical	< 1
Jet energy scale	0.2
Photon energy scale	0.2–0.4
Conversion reconstruction eff.	7–45
Uncertainty at finite $\lvert d_{XY}\rvert$	40

Furthermore, the efficiency for the reconstruction of a conversion photon with finite $|d_{XY}|$ is estimated using simulation. Since there are no suitable control samples in collision data to perform a comparison, we apply a conservative 40% uncertainty on the signal on the basis of how well the tracking efficiencies are predicted by the simulation of the track reconstruction [23]. From Fig. 5 we see that there is a difference in shape between CR2 and CR1. This difference is used as a shape uncertainty on our background estimate. Furthermore, in order to quantify the possible effects of signal contamination in our data control sample we calculate the fraction of the signal events found in our background control region, CR1, with respect to the search region. We find that this quantity never exceeds 1.5%, which is negligible. Lastly, we find the statistical uncertainty of our background estimate is 58%.

8 Results and Interpretation

The number of signal and background events in data are estimated from the binned $|d_{XY}|$ distributions optioned after the selection described in Section 4 and shown in Fig. 6. The distribution for the main background, γ+jet, is derived from the data control samples, as described in Section 6 and the normalisation is set to the first bin in the data $|d_{XY}|$ distribution. The last bin contains also overflows. We tabulate the cut flow for signal, background, and data after various selection cuts in Table 2. The preselection is defined as: passing the trigger; at least one good reconstructed vertex; at least one loosely identified photon.

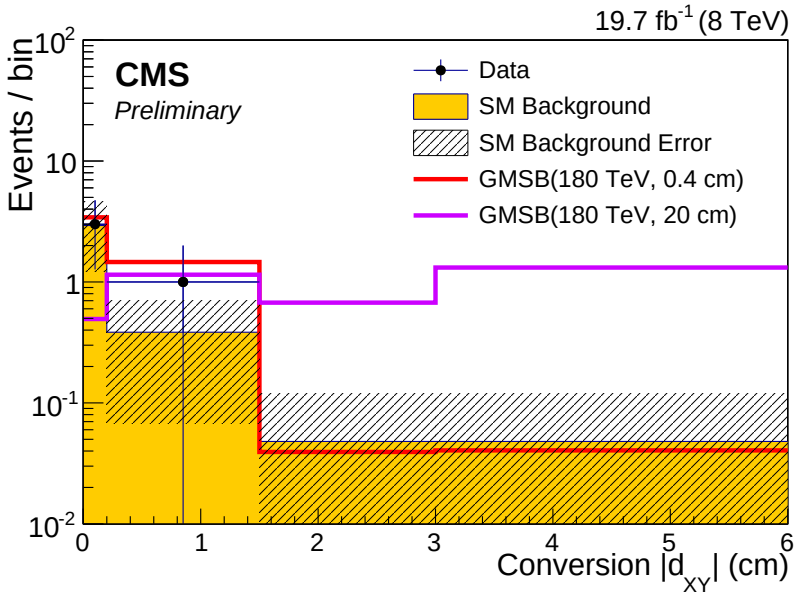

Figure 6: Distribution of $|d_{XY}|$: data are compared with background which is estimated from CR1. Two signal points for $\Lambda = 180$ TeV, of $c\tau = 0.4$ cm and 20 cm are also shown for comparison. The black hatches correspond to the total uncertainty on the background estimate. The last bin for each histogram contains the overflow.

Table 2: Cutflow for signal ($c\tau = 0.4$ cm and $c\tau = 20$ cm) and the expected SM backgrounds.

	GMSB (180, 0.4)	GMSB (180, 20)	SM bkg. estimate (CR1)	Data
All	285	285	-	5.21e+11
Preselection	182	176	-	7.34e+10
$E_T^{miss} > 60$	174	167	-	1.86e+09
Num. jets ≥ 2	102	98	-	4.55e+08
Num. phot. ≥ 2	41	41	-	1.42e+06
Num. conv. ≥ 1	5.0 ± 0.4	3.7 ± 0.8	3.5 ± 2.2	4

There is no significant excess of events in data with respect to the background expectations, therefore we interpret the results of our search in terms of upper limits at 95% confidence level (CL) on the production cross section of a long-lived neutralino in the context of the GMSB model. A test of the background-only and signal+background hypotheses is performed using a modified frequentist approach, often referred to as CL_s [24–26]. The probability distributions of the background-only and the signal+background hypotheses are determined from distributions of the test statistic constructed from pseudo-experiments. Once the ensembles of pseudo-experiments for the two hypotheses are generated, the observed CL_s limit is calculated from these distributions and the actual observation of the test statistic. The expected CL_s limit is calculated by replacing the test statistic by the expected median from the distribution of the background-only hypothesis. The background shape is taken from Fig. 5 and the normalisation is taken from the $|d_{XY}|$ peak of data. Furthermore, since we normalise our background to the first bin of data, we exclude the signal contribution from this bin in the limit setting procedure. The uncertainties are handled by introducing nuisance parameters both on the normalisation and the shape of the signal and background expectations. The results can be seen in Fig. 7. Here we plot the region of GMSB phase space where the observed and expected median CL_s limit falls below the theoretical expectation, and we are therefore able to exclude.

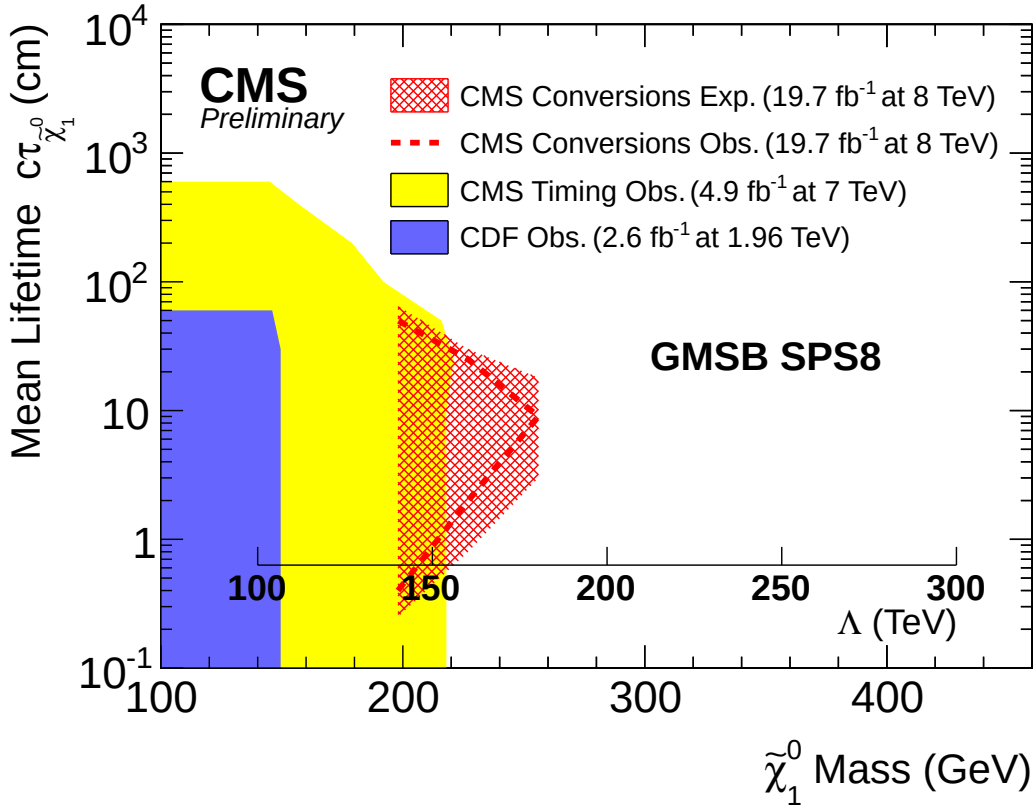

Figure 7: Exclusion plot in the plane defined by the $\tilde{\chi}_1^0$ and its mean lifetime in the context of the SPS8 model of GMSB supersymmetry. The Λ scale is also shown.

9 Summary

This paper described the search for long-lived neutral particles decaying to photons in a sample of data from proton–proton interactions at the center-of-mass energy of 8 TeV collected by CMS at the LHC and corresponding to 19.7 fb^{-1} of integrated luminosity. The GMSB scenario with a long-lived neutralino decaying to photon plus gravitino was used as reference. No significant excess over the expected number of background events has been observed, and 95% CL exclusion limits on the GMSB production cross section have been derived. In this scheme, we obtain an exclusion region as a function of both the neutralino mass and its mean lifetime. The mass of the lightest neutralino is then restricted to values $m(\tilde{\chi}_1^0) > 250\,\text{GeV}$, for mean neutralino lifetime $c\tau = 10\,\text{cm}$. Also, the mean lifetime must be greater than 11 cm, for $m(\tilde{\chi}_1^0) = 160\,\text{GeV}$. Furthermore, we see roughly a factor of 10 improvement with respect to the 7 TeV result.

10 Acknowledgements

We congratulate our colleagues in the CERN accelerator departments for the excellent performance of the LHC and thank the technical and administrative staffs at CERN and at other CMS institutes for their contributions to the success of the CMS effort. In addition, we gratefully acknowledge the computing centres and personnel of the Worldwide LHC Computing Grid for delivering so effectively the computing infrastructure essential to our analyses. Finally, we acknowledge the enduring support for the construction and operation of the LHC and the CMS detector provided by the following funding agencies: BMWFW and FWF (Austria); FNRS and FWO (Belgium); CNPq, CAPES, FAPERJ, and FAPESP (Brazil); MES (Bulgaria); CERN; CAS, MoST, and NSFC (China); COLCIENCIAS (Colombia); MSES and CSF (Croatia); RPF (Cyprus); MoER, ERC IUT and ERDF (Estonia); Academy of Finland, MEC, and HIP (Finland); CEA and CNRS/IN2P3 (France); BMBF, DFG, and HGF (Germany); GSRT (Greece); OTKA and NIH (Hungary); DAE and DST (India); IPM (Iran); SFI (Ireland); INFN (Italy); MSIP and NRF (Republic of Korea); LAS (Lithuania); MOE and UM (Malaysia); CINVESTAV, CONACYT, SEP, and UASLP-FAI (Mexico); MBIE (New Zealand); PAEC (Pakistan); MSHE and NSC (Poland); FCT (Portugal); JINR (Dubna); MON, RosAtom, RAS and RFBR (Russia); MESTD (Serbia); SEIDI and CPAN (Spain); Swiss Funding Agencies (Switzerland); MST (Taipei); ThEPCenter, IPST, STAR and NSTDA (Thailand); TUBITAK and TAEK (Turkey); NASU and SFFR (Ukraine); STFC (United Kingdom); DOE and NSF (USA). Individuals have received support from the Marie-Curie programme and the European Research Council and EPLANET (European Union); the Leventis Foundation; the A. P. Sloan Foundation; the Alexander von Humboldt Foundation; the Belgian Federal Science Policy Office; the Fonds pour la Formation à la Recherche dans l'Industrie et dans l'Agriculture (FRIA-Belgium); the Agentschap voor Innovatie door Wetenschap en Technologie (IWT-Belgium); the Ministry of Education, Youth and Sports (MEYS) of the Czech Republic; the Council of Science and Industrial Research, India; the HOMING PLUS programme of the Foundation for Polish Science, cofinanced from European Union, Regional Development Fund; the Compagnia di San Paolo (Torino); the Consorzio per la Fisica (Trieste); MIUR project 20108T4XTM (Italy); the Thalis and Aristeia programmes cofinanced by EU-ESF and the Greek NSRF; and the National Priorities Research Program by Qatar National Research Fund.

References

[1] M. J. Strassler and K. M. Zurek, "Echoes of a hidden valley at hadron colliders", *Phys. Lett. B* **651** (2007) 374, doi:10.1016/j.physletb.2007.06.055, arXiv:hep-ph/0604261.

[2] G. F. Giudice and R. Rattazzi, "Theories with gauge-mediated supersymmetry breaking", *Phys. Rept.* **322** (1999) 419, doi:10.1016/S0370-1573(99)00042-3, arXiv:hep-ph/9801271.

[3] G. R. Farrar and P. Fayet, "Phenomenology of the production, decay, and detection of new hadronic states associated with supersymmetry", *Phys. Lett. B* **76** (1978) 575, doi:10.1016/0370-2693(78)90858-4.

[4] B. C. Allanach et al., "The Snowmass Points and Slopes: benchmarks for SUSY searches", *Eur. Phys. J. C* **25** (2002) 113, doi:10.1007/s10052-002-0949-3, arXiv:hep-ph/0202233.

[5] S. Dimopoulos, M. Dine, S. Raby, and S. D. Thomas, "Experimental signatures of low-energy gauge mediated supersymmetry breaking", *Phys. Rev. Lett.* **76** (1996) 3494, doi:10.1103/PhysRevLett.76.3494, arXiv:hep-ph/9601367.

[6] "CMS Twiki",. https://twiki.cern.ch/twiki/bin/view/CMSPublic/PhysicsResultsSUS.

[7] D0 Collaboration, "Search for long-lived particles decaying into electron or photon pairs with the D0 detector", *Phys.Rev.Lett.* **101** (2008) 111802, doi:10.1103/PhysRevLett.101.111802, arXiv:0806.2223.

[8] ATLAS Collaboration, "Search for nonpointing photons in the diphoton and E_T^{miss} final state in $\sqrt{s}$=7TeV proton-proton collisions using the ATLAS detector", *Phys.Rev.* **D88** (2013), no. 1, 012001, doi:10.1103/PhysRevD.88.012001, arXiv:1304.6310.

[9] ATLAS Collaboration, "Search for nonpointing and delayed photons in the diphoton and missing transverse momentum final state in 8 TeV pp collisions at the LHC using the ATLAS detector", *Phys.Rev.* **D90** (2014), no. 11, 112005, doi:10.1103/PhysRevD.90.112005, arXiv:1409.5542.

[10] CDF Collaboration, "Search for heavy, long-lived particles that decay to photons at CDF II", *Phys.Rev.Lett.* **99** (2007) 121801, doi:10.1103/PhysRevLett.99.121801, arXiv:0704.0760.

[11] CMS Collaboration, "Search for long-lived particles decaying to photons and missing energy in proton-proton collisions at $\sqrt{s} = 7$ TeV", *Phys.Lett.* **B722** (2013) 273–294, doi:10.1016/j.physletb.2013.04.027, arXiv:1212.1838.

[12] CMS Collaboration, "Search for new physics with long-lived particles decaying to photons and missing energy in pp collisions at $\sqrt{s} = 7$ TeV", *JHEP* **1211** (2012) 172, doi:10.1007/JHEP11(2012)172, arXiv:1207.0627.

[13] CMS Collaboration, "The CMS experiment at the CERN LHC", *JINST* **3** (2008) S08004, doi:10.1088/1748-0221/3/08/S08004.

[14] CMS Collaboration, "Energy Calibration and Resolution of the CMS Electromagnetic Calorimeter in pp Collisions at $\sqrt{s} = 7$ TeV", *JINST* **8** (2013) P09009, doi:10.1088/1748-0221/8/09/P09009, arXiv:1306.2016.

[15] CMS Collaboration, "Description and performance of track and primary-vertex reconstruction with the CMS tracker", *JINST* **9** (2014), no. 10, P10009, doi:10.1088/1748-0221/9/10/P10009, arXiv:1405.6569.

[16] T. Sjostrand, S. Mrenna, and P. Z. Skands, "PYTHIA 6.4 Physics and Manual", *JHEP* **0605** (2006) 026, doi:10.1088/1126-6708/2006/05/026, arXiv:hep-ph/0603175.

[17] GEANT4 Collaboration, "GEANT4: A Simulation toolkit", *Nucl.Instrum.Meth.* **A506** (2003) 250–303, doi:10.1016/S0168-9002(03)01368-8.

[18] M. Cacciari, G. P. Salam, and G. Soyez, "The Anti-k(t) jet clustering algorithm", *JHEP* **0804** (2008) 063, doi:10.1088/1126-6708/2008/04/063, arXiv:0802.1189.

[19] CMS Collaboration, "Performance of photon reconstruction and identification with the CMS detector in proton-proton collisions at $\sqrt{s}$ = 8 TeV", arXiv:1502.02702.

[20] CMS Collaboration, "Jet Performance in pp Collisions at 7 TeV", Technical Report CMS-PAS-JME-10-003, CERN, Geneva, 2010.

[21] CMS Collaboration, "Searches for electroweak neutralino and chargino production in channels with Higgs, Z, and W bosons in pp collisions at 8 TeV", *Phys.Rev.* **D90** (2014) 092007, doi:10.1103/PhysRevD.90.092007, arXiv:1409.3168.

[22] CMS Collaboration, "Absolute Calibration of the Luminosity Measurement at CMS: Winter 2012 Update", Technical Report CMS-PAS-SMP-12-008, CERN, Geneva, 2012.

[23] CMS Collaboration, "Description and performance of track and primary-vertex reconstruction with the CMS tracker", *JINST* **9** (2014), no. 10, P10009, doi:10.1088/1748-0221/9/10/P10009, arXiv:1405.6569.

[24] The ATLAS Collaboration, The CMS Collaboration, The LHC Higgs Combination Group Collaboration, "Procedure for the LHC Higgs boson search combination in Summer 2011", Technical Report CMS-NOTE-2011-005. ATL-PHYS-PUB-2011-11, CERN, Geneva, Aug, 2011.

[25] T. Junk, "Confidence level computation for combining searches with small statistics", *Nucl.Instrum.Meth.* **A434** (1999) 435–443, doi:10.1016/S0168-9002(99)00498-2, arXiv:hep-ex/9902006.

[26] A. L. Read, "Presentation of search results: the CL s technique", *Journal of Physics G: Nuclear and Particle Physics* **28** (2002), no. 10, 2693.